Phys Chem Minerals (2000) 27: 747–756

ORIGINAL PAPER

R. L. Withers · Y. Tabira · J. A. Valgoma · M. Aroyo
M. T. Dove

The inherent displacive flexibility of the hexacelsian tetrahedral framework and its relationship to polymorphism in Ba-hexacelsian

Received: 30 December 1999 / Accepted: 16 May 2000

Abstract The results of a rigid unit mode (RUM) analysis of the inherent displacive structural flexibility of the tetrahedral framework of the ideal hexacelsian structure type are presented. One of the three types of RUM found to exist is characterized by modulation wave vectors perpendicular to $\langle 110 \rangle$ and atomic displacement patterns involving tetrahedral rotation around the parent c axis while a second type of RUM is found to be soft at any modulation wave vector and to involve tetrahedral rotation about in-plane rotation axes. It is shown how a combination of these two types of RUM motion associated with the same $\mathbf{q} = 1/2\langle \bar{1}101 \rangle^*$ modulation wave vector enables the outstanding crystal chemical problems and apparently mutually contradictory results as regards polymorphism in Ba-hexacelsian to be resolved.

Key words Hexacelsian · Phase transition · Diffuse distribution · Dynamical disorder · Correlated tetrahedral rotation

Introduction

The exact nature of the α and β phases of Ba-hexacelsian ($BaAl_2Si_2O_8$), as well as the structural origin of the $\sim$310 °C α to β phase transition therein, have long been problematic (Ito 1950; Takéuchi 1958; Oehlschlegel et al. 1974, 1976; Pentinghaus 1975; Müller 1977; Kremenovic et al. 1997, 1999; Tabira et al. 2000). The underlying $P6/mmm$ ($a_p \sim 5.3$ Å, $c_p \sim 7.8$ Å, p for parent) average structure (see Fig. 1) with its characteristic double tetrahedral layers of corner-connected TO_4 ($T = Al_{0.5}Si_{0.5}$) tetrahedra interspersed with layers of Ba ions was first established by Ito (1950). Problems with ascribing this simple, highly symmetric "average" or parent structure to the α phase, however, were immediately apparent. They include the absence of (expected) Al/Si ordering, unrealistically short T-O bond distances and Ba-O bond distances that are too long (reflected in calculated bond valence sums – see Table 1a), linear T-O-T bond angles along the c_p axis and the lack of a reasonable explanation for the existence of the α to β phase transition itself.

Consequently, Takéuchi (1958) reinvestigated, using the same apparent single crystal as that used earlier by Ito 1950, and discovered the existence of weak additional satellite reflections of the type $\mathbf{G} \pm 1/2\langle \bar{1}101 \rangle^*$ (**G** refers to the strong Bragg reflections of the underlying parent structure) in the room temperature α phase which apparently disappeared at the α to β phase transition. Despite the absence of any orthorhombic strain distortion of the underlying metric, Takéuchi (1958) correctly deduced that the observed reciprocal lattice was a triply twinned composite of individual body centred orthorhombic lattices (I—, $a_o = a_p$, $b_o = \sqrt{3}a_p$, $c_o = 2c_p$) corresponding to a single condensed mode of $1/2\langle \bar{1}101 \rangle^*$ type. [This has subsequently been confirmed by means of both satellite dark field imaging (Müller 1977) and microdiffraction (Tabira et al. 2000).] The α to β phase transition at $\sim$310 °C was thus attributed to an I— ($a_o = a_p$, $b_o = \sqrt{3}a_p$, $c_o = 2c_p$) to $P6/mmm$ (a_p, c_p) phase transition. Takéuchi (1958) further attempted to "..deduce... the atomic positions... in an orthorhombic individual..." via a difference Fourier analysis of the average structure. Evidence was thereby found for an apparent reduction in the symmetry of individual layers from hexagonal to trigonal via tetrahedral rotation of individual TO_4 tetrahedra around c_p (see, for example,

R. L. Withers (✉) · Y. Tabira
Research School of Chemistry,
Australian National University,
Canberra, ACT, 0200, Australia
e-mail: withers@rsc.anu.edu.au
Fax: +61 2 62490750

J. A. Valgoma · M. Aroyo
Departamento de Fisica de la Materia Condensada,
Universidad del Pais Vasco, Bilbao, Spain

M. T. Dove
Department of Earth Sciences,
University of Cambridge, Downing Street,
Cambridge CB2 3EQ, UK

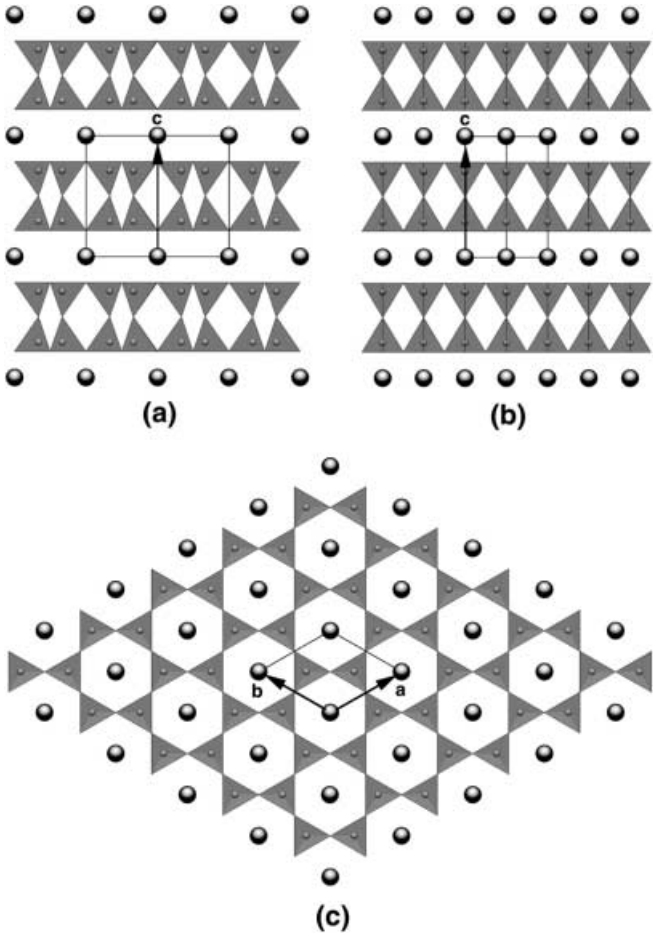

Fig. 1a–c The P6/*mmm* ideal hexacelsian tetrahedral framework structure is shown in projection down a $\langle 110 \rangle$ direction in **a**, a $\langle 1\bar{1}0 \rangle$ direction in **b** and the [001] direction in **c**. The *large filled circles* are the Ba ions while the *smaller filled circles* represent the Al, Si ions. The projected parent unit cell is outlined in **a**, **b** and **c**. Note the double tetrahedral layers of corner-connected (Al, Si)O_4 tetrahedra interspersed with layers of Ba ions characteristic of the hexacelsian framework topology

Table 1 a Calculated bond valence sums (AVs) for the ideal *P*6/*mmm* parent structure

	Ba	T	O(1)	O(2)
AV (T = Al)	1.233	4.166	2.114	2.278
AV (T = Si)	1.233	3.873	1.965	2.132
Average AV	1.233	4.020	2.040	2.205
Expected AV	2.0	3.5	2.0	2.0

Coordinates from Table 2 of Takéuchi (1958) with the O(2) x coordinate taken as 1/2. Bond valence parameters from Brese and O'Keeffe 1991

b Calculated bond valence sums (AVs) for the $P\bar{3}$ structure of α-hexacelsian$_{LTA}$

	Ba	Al	Si	O(1)	O(2)
AV	1.590	3.162	4.232	2.278	2.071
Expected AV	2.0	3.0	4.0	2.0	2.0

Coordinates from Table 2 of Kremenovic et al. 1997

Fig. 2a) and interpreted in terms of a specific sequence of such trigonal type layers (see Fig. 15 of Takéuchi 1958; Takéuchi and Donnay 1959). The problem with this latter interpretation, however, is that it can only give rise to satellite reflections of $\mathbf{G} \pm 1/2[0001]^*$ type and never of the observed $\mathbf{G} \pm 1/2\langle\bar{1}101\rangle^*$ type.

Matters were subsequently complicated still further by the largely TEM study of Müller (1977), who reported the intimate coexistence of two distinct hexacelsian polymorphs at room temperature, a $P6_3/mcm$, $a = a_p$, $c = 2c_p$ polymorph and an *Immm*, $a_o = a_p$, $b_o = \sqrt{3}a_p$, $c_o = 2c_p$ polymorph. The former polymorph is known to exist for $CaAl_2Si_2O_8$ (Takéuchi and Donnay 1959) and $SrAl_2Si_2O_8$ (Schadt et al. 1976; Toepel-Schadt et al. 1978) but had not previously been reported for $BaAl_2Si_2O_8$. The latter polymorph was presumed to be the same as that described by Takéuchi (1958). The room temperature coexistence of the two distinct hexacelsian

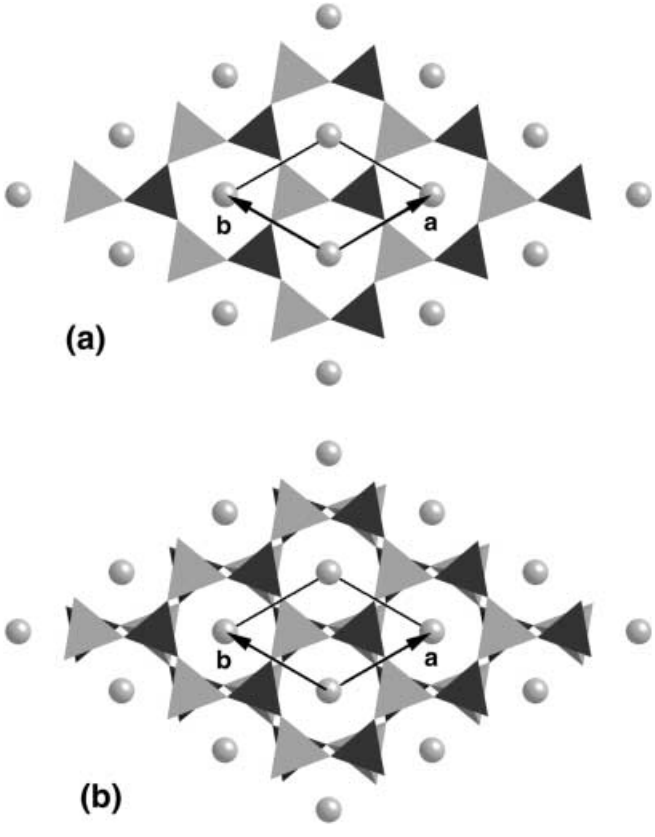

Fig. 2 An [001] projection of the $P\bar{3}(a = a_p, c = c_p)$, Al/Si ordered crystal structure of room temperature Ba-hexacelsian recently reported by Kremenovic et al. (1997). The smaller SiO_4 tetrahedra are shown in *black*, the larger AlO_4 tetrahedra in *grey* and the Ba atoms are represented by the *large grey balls*. A single tetrahedral layer is shown in **a** and both tetrahedral layers per unit cell in **b**. The deviation of the refined crystal structure from the underlying *P*6/*mmm* parent structure can be described in terms of condensed $\mathbf{q} = \mathbf{0}$ modes involving (1) Al/Si ordering and correlated expansion/reduction of the size of the associated TO_4 tetrahedra and (2) correlated tetrahedral rotation of individual $Al_2Si_2O_8$ layers about c_p leading to a reduction in the symmetry of individual layers from hexagonal to trigonal and characteristic di-trigonal cavities (see **a**)

polymorphs was attributed to differences in local chemical composition (it is known that it is possible to prepare off ideal stoichiometry $Ba_{1-x}Al_{2-2x}Si_{2+2x}O_8$ hexacelsians over significant composition ranges, e.g. $0.00 < x < 0.15$ (Oehlschlegel et al. 1974, 1976; Kremenovic et al. 1997) and brings into doubt the equilibrium nature of the synthesized specimens studied. In a TEM heating stage, the $P6_3/mcm$ polymorph was found to invert to the *Immm* polymorph when heated. Müller (1977) thus concluded that the $P6_3/mcm$ polymorph was the stable room temperature polymorph for exactly stoichiometric $BaAl_2Si_2O_8$ and that the ~300 °C α to β phase transition therein was due to a $P6_3/mcm$ to *Immm* phase transition. The observed existence of twin and antiphase domains in the *Immm* polymorph was further interpreted as a signature of a yet higher temperature subsolidus phase transition, this time from *Immm* to $P6/mmm$.

More recently still, Kremenovic and colleagues (Dondur et al. 1995; Dimitrijevic et al. 1997; Kremenovic et al. 1997, 1999) have extensively investigated both stoichiometric and non-stoichiometric Ba-hexacelsians synthesized from zeolite precursors. ^{29}Si MAS NMR spectra of the stoichiometric material at room temperature showed, for the first time, an ordered Si(4Al) tetrahedral environment in the double tetrahedral sheets in agreement with Loewenstein's rule (Loewenstein 1954). (Note that such Al/Si ordering can only be compatible with either a $\mathbf{q} = \mathbf{0}$ or a $\mathbf{q} = 1/2\mathbf{c}^*$ compositional modulation wave but not with a $\mathbf{q} = 1/2[\bar{1}101]^*$ compositional modulation wave). The same stoichiometric material was also shown to undergo the α to β phase transition at ~310 °C whereas the nonstoichiometric specimen did not. A time-resolved synchrotron XRPD refinement (Kremenovic et al. 1997) of both the α and β phases of the stoichiometric hexacelsian specimen again found evidence for tetrahedral rotation around c_p but this time reported $P\bar{3}$ ($a = a_p$, $c = c_p$) space group symmetry on either side of the phase transition. Such a unit cell implies that no additional satellite reflections were detected.

The deviation of the Kremenovic et al. (1997) refined crystal structures from the underlying $P6/mmm$ parent structure can be described in terms of condensed $\mathbf{q} = \mathbf{0}$ modes involving (1) Al/Si ordering and correlated expansion/reduction of the size of the associated TO_4 tetrahedra and (2) correlated tetrahedral rotation of individual $Al_2Si_2O_8$ layers about c_p leading to a reduction in the symmetry of individual layers from hexagonal to trigonal (see Fig. 2a). The results of Kremenovic et al. (1997) are quite compatible with the difference Fourier analysis of the average structure reported by Takéuchi (1958) in the sense that trigonal individual layers are formed (see Fig. 2a). It differs, however, in the proposed sequence of these trigonal layers (cf. Fig. 2b with Fig. 15 of Takéuchi 1958). While the Kremenovic et al. (1997) reported crystal structures for both the α and β phases significantly improve the local crystal chemistry with respect to the original $P6/mmm$ model (cf. Table 1b with Table 1a), problems still remain, i.e. Ba is still significantly underbonded while Al and Si are still significantly overbonded. In addition, linear T-O-T bond angles (along the c_p axis) also still remain. Perhaps the major problem remaining, however, is that there is still no indication as to the structural origin of the $\mathbf{G} \pm 1/2\langle\bar{1}101\rangle^*$ type satellite reflections first reported as existing in the α phase by Takéuchi (1958) and recently reconfirmed (via a temperature-dependent electron diffraction study) as existing in both the α and β phases (see Fig. 3 and Tabira et al. 2000).

The purpose of the current paper is, firstly, to present the results of a rigid unit mode (RUM) analysis of the inherent displacive structural flexibility of the tetrahedral framework of the ideal hexacelsian structure type and, secondly, to show how the existence of two quite distinct types of RUM (one involving tetrahedral rotation around c_p and the other tetrahedral rotation about in-plane rotation axes) might enable the outstanding crystal chemical problems and apparently mutually contradictory results as regards polymorphism in Ba-hexacelsian to be resolved.

RUMs of the ideal hexacelsian structure type

The two-dimensional tetrahedral framework of the ideal $P6/mmm$ hexacelsian structure type (see Fig. 1) is inherently flexible as a result of the existence of low (essentially zero) frequency modes of distortion which do not distort the constituent TO_4 tetrahedra but which result in changes in their relative orientation. The energies associated with deformation of these TO_4 tetrahedral units are typically much larger than the energies associated with rotation of neighbouring tetrahedral units about a common vertex atom (Hammonds et al. 1996; Dove et al. 1998; Thompson et al. 1998a, b) or the energies associated with the bonding interactions between the oxygens of the tetrahedra and the interstitial Ba ions. Consequently, only those modes of distortion of this tetrahedral framework which entail zero or minimal distortion of these rigid polyhedral units (rigid unit modes or RUMs) can reasonably be expected to occur in response to lowering of temperature and hence to be responsible for low temperature phase transitions and polymorphism in hexacelsians. The recently developed lattice dynamics program CRUSH (Hammonds et al. 1994) enables the existence of such zero frequency RUM modes to be easily detected.

RUMs of Type I

Direct experimental evidence for the existence of one such type of RUM, in the form of transverse polarized diffuse sheets of intensity perpendicular to $\langle 110\rangle$ real space directions and giving rise to intense diffuse streaking along $\langle \bar{h}h0l\rangle^*$ directions of reciprocal space (see, for example, Fig. 3), has recently been shown to be

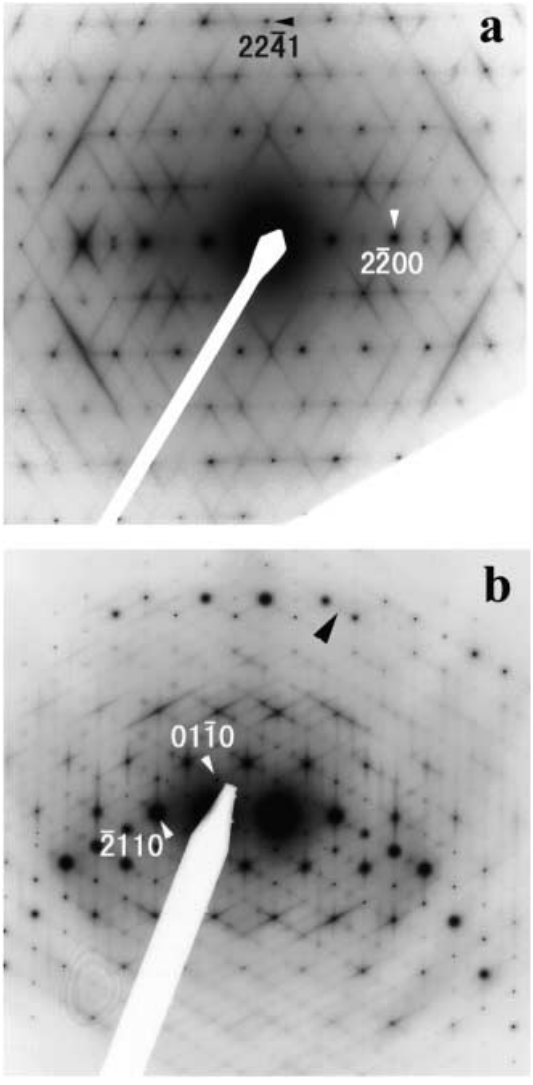

Fig. 3a $\langle 114 \rangle$ and **b** close to [001] zone axis selected area diffraction patterns (SADPs) of $BaAl_2Si_2O_8$ upon heating above the ~312 °C phase transition in a TEM heating stage. Note the strong and characteristic diffuse intensity distribution in the form of transverse polarized diffuse streaking along all $\langle \bar{h}h0l \rangle^*$ directions of reciprocal space in both **a** and **b** as well as the continued existence of satellite reflections of the type $\mathbf{G} \pm 1/2\langle \bar{1}101 \rangle^*$ (**G** refers to the strong Bragg reflections of the underlying parent structure) above the α to β phase transition (the two satellite reflections to *either side of the dark arrow* in **b**, for example, correspond to two particular such $\mathbf{G} \pm 1/2\langle \bar{1}101 \rangle^*$ type satellite reflections). SADPs and zone axis orientations have been indexed with respect to the underlying P6/*mmm* hexagonal parent structure shown in Fig. 1

characteristic of the high-temperature β phase of Ba-hexacelsian. Indeed, the quite reproducible appearance and disappearance of this characteristic diffuse intensity distribution on cycling up and down through the ~310 °C α to β phase transition was found to be the defining characteristic of the phase transition itself (Tabira et al. 2000).

The localized nature of the soft modulation wave vectors involved (perpendicular to $\langle 110 \rangle$ real space directions), in conjunction with the transverse polarized character of the sheets of diffuse intensity (see Fig. 3), enabled the associated atomic displacement pattern responsible to be deduced (Tabira et al. 2000), as shown in Fig. 4a. RUMs of this type can be attributed to coupled (along $\langle 110 \rangle$) tetrahedral rotations of $\langle 110 \rangle$ columns of tetrahedra (uncorrelated from column to column as a result of the rotation axes running through the O(2) oxygen ions linking neighbouring columns) around the $\mathbf{c}_p$ axis (see Fig. 4a). Note that the resultant pattern of atomic displacements within any one $\langle 110 \rangle$ column can be decomposed into rotations of the tetrahedra about $\mathbf{c}_p$ through the centre of the tetrahedra coupled with a rigid

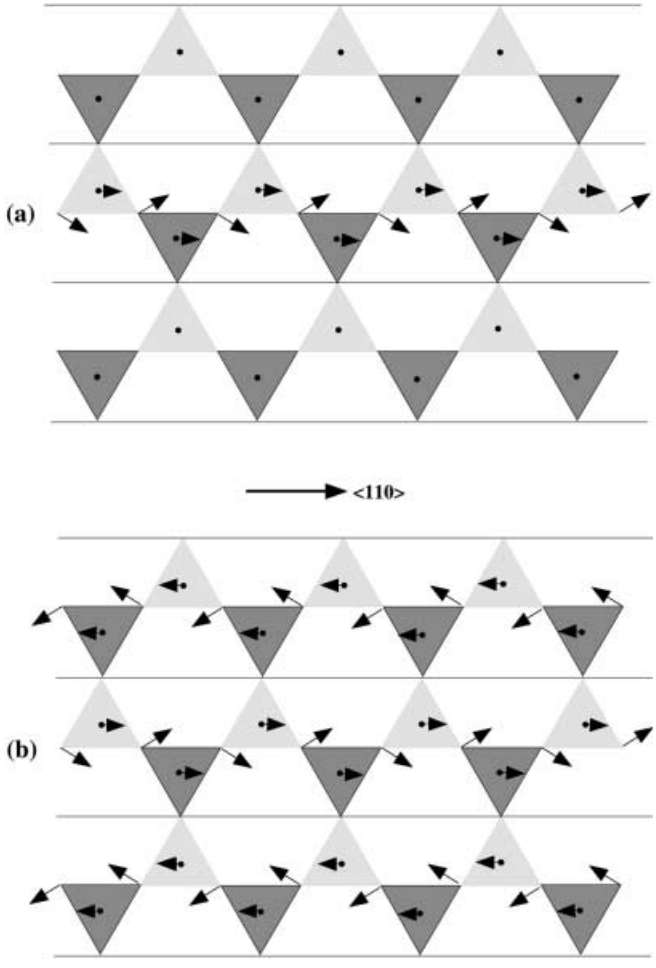

Fig. 4 a [001] projection of a two tetrahedral layer slab of ideal hexacelsian showing the correlated tetrahedral rotations (of $\langle 110 \rangle$ columns of tetrahedra) characteristic of the first type of RUM and responsible for the observed high-temperature diffuse distribution (see Fig. 3). Three such $\langle 110 \rangle$ columns are shown with neighbouring columns separated by the *full lines*. Note that the sense of rotation in going from one column to the next across the full lines is undetermined, i.e. the tetrahedral rotations are uncorrelated from column to column as a result of the rotation axes running through the O(2) oxygen ions linking neighbouring columns. **b** shows the particular rotation pattern in one two-layer tetrahedral slab resulting from a condensed RUM of this type characterized by the modulation wave vector $\mathbf{q} = 1/2[\bar{1}101]^*$. The $1/2\mathbf{c}^*$ component of this modulation wave vector implies that the sense of the atomic displacements shown will be reversed in the next two-layer slab

body transverse displacive shift of each tetrahedra along $\langle 110\rangle$. [A condensed $\mathbf{q} = 1/2\ [0001]^*$ RUM of this type (see, for example, Fig. 2a and Fig. 6 of Takéuchi and Donnay 1959) gives rise to the reported Ca- and Sr-hexacelsian low temperature polymorphs (Takéuchi and Donnay 1959)]. The resultant displacement pattern associated with a $\mathbf{q} = 1/2[\bar{1}101]^*$ RUM of this type is shown in Fig. 4b (for one particular double tetrahedral layer). Analysis of the CRUSH output for the ideal hexacelsian framework structure has confirmed the existence of this first type of RUM distortion.

RUMs of Type II

In addition, however, it has shown the existence of a second quite distinct type of RUM which is, rather remarkably, soft at any particular modulation wave vector. Unfortunately, this time it is not so easy to interpret the output of CRUSH in terms of associated displacement eigenvectors. Careful analysis shows that the atomic displacement pattern associated with this type of RUM again entails tetrahedral rotation, but this time about an in-plane rotation axis running through the basal planes of the tetrahedra themselves (see, for example, Fig. 5). The existence of a second type of RUM of this sort is particularly important in the case of hexacelsians in that it is only distortions of this type, i.e. involving basal plane rotation axes, that can give rise to non-linear T-O-T bond angles along the c_p axis, which seems to be an almost inviolable crystal chemical rule for silicates and alumino-silicates (Gibbs et al. 1981; Liebau 1985).

The in-plane direction of the rotation axis for this second type of RUM, however, does not always run along $\langle \bar{1}10\rangle$ real space directions (as is the case in Fig. 5) but is sensitively dependent upon the choice made for the h and k indices of the particular $\mathbf{q} = [hkl]^*(= h\mathbf{a}^* + k\mathbf{b}^* + l\mathbf{c}^*)$ modulation wave vector chosen. It is not difficult to see from a comparison of Figs. 5, 4a and 1c that a RUM of the sort shown in Fig. 5, i.e. involving basal plane rotation about a $\langle \bar{1}10\rangle$ axis (labelled R_y in what follows, see Fig. 6), is to be expected for any modulation wave vector perpendicular to $\langle 110\rangle$, i.e. of $\langle \bar{h}h01\rangle^*$ type. For a general modulation wave vector, however, an additional orthogonal basal plane rotation axis must be considered. This additional rotation axis runs along the orthogonal $\langle 110\rangle$ direction (labelled R_x in what follows, see Fig. 6). Both rotation axes run through the point defined by the projection of the local T atom onto the relevant tetrahedral basal plane (see, for example, the $\langle \bar{1}10\rangle$ rotation axis marked by the asterix in Fig. 5). The in-plane direction of the rotation axis for a particular tetrahedron then depends upon the relative magnitude of $R_x \exp(i\theta_x)$ and $R_y \exp(i\theta_y)$ for that particular tetrahedron [see Fig. 6 and Eq. (1) below].

Consider, for example, the four independent tetrahedra per parent unit cell which we label T_1 to T_4 in Fig. 6 (tetrahedra T_1 and T_3 are understood to be pointing up in Fig. 6 with the tetrahedra immediately above them, T_2 and T_4, understood to be pointing down). Now consider the constraints on the amplitudes (R_x, R_y) and phases (θ_x, θ_y) of the local rotations imposed by the topological connectivity of the ideal hexacelsian framework structure and the requirement that oxygens linking neighbouring tetrahedra should not split. We write the local (anticlockwise) rotations of tetrahedra T_n in unit cell $\mathbf{t}$ as:

$$R_{Tn}(\mathbf{t}) = R_{xn}\cos[-2\pi\mathbf{q}\cdot\mathbf{t} + \theta_{xn}] + R_{yn}\cos[-2\pi\mathbf{q}\cdot\mathbf{t} + \theta_{yn}]\ . \quad (1)$$

Consider, for example, the apical oxygens linking tetrahedra T_1 and T_2 as well as tetrahedra T_3 and T_4. The constraint that these apical oxygen atoms should not split is equivalent to the requirement that

$$R_{x2} = -R_{x1}, \theta_{x2} = \theta_{x1} \quad \text{and} \quad R_{y2} = -R_{y1}, \theta_{y2} = \theta_{y1}$$
$$R_{x4} = -R_{x3}, \theta_{x4} = \theta_{x3} \quad \text{and} \quad R_{y4} = -R_{y3}, \theta_{y4} = \theta_{y3}\ , \quad (2)$$

respectively. Thus the rotations of tetrahedra T_2 and T_4 are completely determined by the rotations of tetrahedra

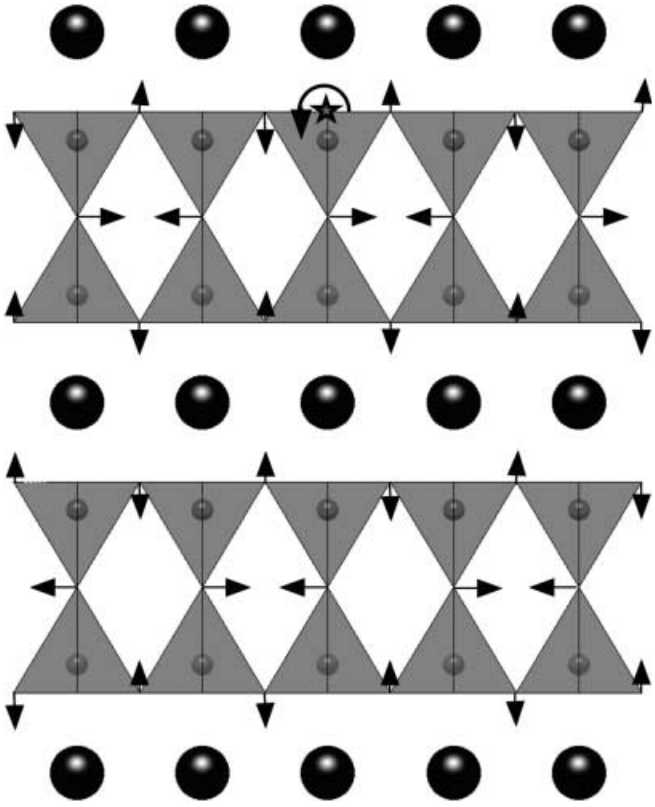

Fig. 5 A $\langle 1\bar{1}0\rangle$ projection of the correlated tetrahedral rotations around $\langle 1\bar{1}0\rangle$ associated with a $\mathbf{q} = 1/2[\bar{1}101]^*$ RUM of type II. The rotation axes run along the $\langle 1\bar{1}0\rangle$ direction through the basal plane of the tetrahedra (marked with the *asterisk* on one tetrahedra). To avoid overcrowding, the atomic shifts of the T atoms along $\langle 110\rangle$ due to the tetrahedral rotations have not been shown, i.e. only the atomic shifts of the tetrahedral oxygen atoms have been shown

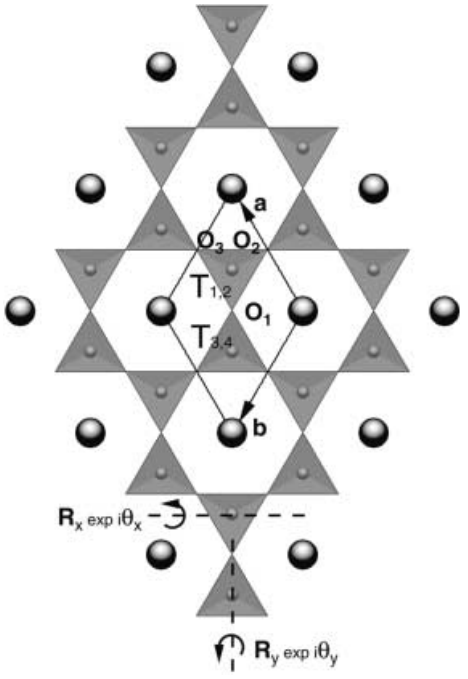

Fig. 6 An [0001] projection of the ideal *P6/mmm* parent structure showing the four independent tetrahedra per parent unit cell which are labelled T_1 to T_4. Tetrahedras T_1 and T_3 are understood to be pointing up with the tetrahedra immediately above them, T_2 and T_4, understood to be pointing down. The *dashed lines* show the *x* and *y* rotation axes running through the basal planes of each tetrahedra

T_1 and T_3 immediately below them and it is therefore on the latter that we now concentrate.

Next consider the constraints imposed by the basal plane oxygens linking tetrahedra T_1 and T_3 (labelled O1, O2 and O3 in Fig. 6). Firstly, consider O1. The constraint that this basal plane oxygen atom should not split requires that

$$R_{x3} = -R_{x1} = -R_x \quad \text{and} \quad \theta_{x3} = \theta_{x1} = \theta_x \ . \tag{3}$$

There is thus one amplitude and one phase degree of freedom remaining as far as rotation around x (or $\langle 110\rangle$) is concerned. Rotation around y (or $\langle \bar{1}10\rangle$), however, does not cause O1 to move and hence does not give rise to a phase relationship between θ_{y1} and θ_{y3}. Time-reversal symmetry, however, requires that $|R_{y1}| = |R_{y3}| = R_y$. Thus we have

$$\begin{aligned} R_{T1}(\mathbf{t}) &= R_x \cos[-2\pi\mathbf{q}\cdot\mathbf{t} + \theta_x] + R_y \cos[-2\pi\mathbf{q}\cdot\mathbf{t} + \theta_{y1}] \\ R_{T3}(\mathbf{t}) &= -R_x \cos[-2\pi\mathbf{q}\cdot\mathbf{t} + \theta_x] \\ &\quad + R_y \cos[-2\pi\mathbf{q}\cdot\mathbf{t} + \theta_{y3}] \ . \end{aligned} \tag{4}$$

At this stage there remain five degrees of freedom (R_x, R_y, θ_x, θ_{y1} and θ_{y3}) and two further oxygen atoms to be taken into account. (Note that one amplitude and one phase degree of freedom must remain undetermined after all constraints have been taken into account for the corresponding atomic displacement pattern to be a RUM).

Now consider oxygen atom O2 (see Fig. 6). O2 belongs simultaneously to tetrahedra T_1 in unit cell (**t**) as well as to tetrahedra T_3 in unit cell (**t** − **b**). Rotation around x and y both cause O2 to displace along **c**. The magnitude and sense of this shift along **c** must then be the same if it is calculated using tetrahedra T_1 in unit cell (**t**) or tetrahedra T_3 in unit cell (**t** − **b**). Hence the constraint that O2 should not split is equivalent to the equality

$$\begin{aligned} &-R_x \cos[-2\pi\mathbf{q}\cdot\mathbf{t} + \theta_x] + \sqrt{3}R_y \cos[-2\pi\mathbf{q}\cdot\mathbf{t} + \theta_{y1}] \\ &\quad = -R_x \cos[-2\pi\mathbf{q}\cdot(\mathbf{t}-\mathbf{b}) + \theta_x] \\ &\qquad - \sqrt{3}R_y \cos[-2\pi\mathbf{q}\cdot(\mathbf{t}-\mathbf{b}) + \theta_{y3}] \ , \end{aligned}$$

where $\mathbf{q} = h\mathbf{a}^* + k\mathbf{b}^* + l\mathbf{c}^*$. Now for the displacement pattern to be a RUM, this constraint must be true for all **t**. Expanding both sides of the above equation in $\cos[-2\pi\mathbf{q}\cdot\mathbf{t}]$ and $\sin[-2\pi\mathbf{q}\cdot\mathbf{t}]$ terms and equating each separately gives rise to the two following (unit cell independent) constraints:

$$\begin{aligned} &-R_x \cos\theta_x + \sqrt{3}R_y \cos\theta_{y1} \\ &\quad = -R_x \cos[\theta_x + 2\pi k] - \sqrt{3}R_y \cos[\theta_{y3} + 2\pi k] \ . \end{aligned} \tag{5}$$

$$\begin{aligned} &-R_x \sin\theta_x + \sqrt{3}R_y \sin\theta_{y1} \\ &\quad = -R_x \sin[\theta_x + 2\pi k] - \sqrt{3}R_y \sin[\theta_{y3} + 2\pi k] \ . \end{aligned} \tag{6}$$

Finally, consider oxygen atom O3. This oxygen belongs simultaneously to tetrahedra T_1 in unit cell (**t**) as well as to tetrahedra T_3 in unit cell (**t** + **a**) (see Fig. 6). The constraint that O3 should not split is therefore equivalent to the equality

$$\begin{aligned} &-R_x \cos[-2\pi\mathbf{q}\cdot\mathbf{t} + \theta_x] - \sqrt{3}R_y \cos[-2\pi\mathbf{q}\cdot\mathbf{t} + \theta_{y1}] \\ &\quad = -R_x \cos[-2\pi\mathbf{q}\cdot(\mathbf{t}+\mathbf{a}) + \theta_x] \\ &\qquad + \sqrt{3}R_y \cos[-2\pi\mathbf{q}\cdot(\mathbf{t}+\mathbf{a}) + \theta_{y3}] \ . \end{aligned}$$

Again, for the displacement pattern to be a RUM, this constraint must be true for all **t**, thus giving rise to the two final additional constraints:

$$\begin{aligned} &-R_x \cos\theta_x - \sqrt{3}R_y \cos\theta_{y1} \\ &\quad = -R_x \cos[\theta_x - 2\pi h] + \sqrt{3}R_y \cos[\theta_{y3} - 2\pi h] \ . \end{aligned} \tag{7}$$

$$\begin{aligned} &-R_x \sin\theta_x - \sqrt{3}R_y \sin\theta_{y1} \\ &\quad = -R_x \sin[\theta_x - 2\pi h] + \sqrt{3}R_y \sin[\theta_{y3} - 2\pi h] \ . \end{aligned} \tag{8}$$

Careful reduction of Eqs. (5) to (8) shows that one of the above four constraints is redundant, leaving three independent constraints and two free variables. The general analytical solution to Eqs. (5) to (8) is

$$\begin{aligned} \theta_{y1} &= \theta_x + 90^\circ + \tan^{-1}[1/2(\cot\pi h - \cot\pi k)] \\ \theta_{y3} &= \theta_x + 90^\circ - \tan^{-1}[1/2(\cot\pi h - \cot\pi k)] \\ R_x/R_y &= \sqrt{3} \times 1/2(\cot\pi h + \cot\pi k) \\ &\quad \times \cos(\tan^{-1}[1/2(\cot\pi h - \cot\pi k)]) \ . \end{aligned} \tag{9}$$

Substitution of Eq. (9) into Eq. (4) then gives an analytical expression (for any general modulation wave

vector) of the local rotation of tetrahedras T_1 and T_3 in any unit cell (**t**) in terms of R_y and θ_x, the two necessarily remaining free variables. The use of Eq. (2) gives the corresponding expressions for tetrahedra T_2 and T_4. Careful consideration of the CRUSH output confirms the validity of the above analytical expressions. In the case of a $\mathbf{q} = 1/2[\bar{1}101]^*$ RUM of this type, note that Eq. (9) predicts $R_x/R_y = 0$ and an in-plane direction of the rotation axis along the $[\bar{1}10]$ direction. The corresponding particularly simple resultant pattern of atomic shifts is shown in Fig. 5.

RUMs of Type III

The $\mathbf{q} = \mathbf{0}$ mode of the type proposed by Kremenovic et al. (1997) (see Fig. 2b) is, in fact, an example of a third type of RUM which is this time localized to modulation wave vectors along the c^* directions of reciprocal space. This type of RUM is (as for RUMs of type I) again characterized by rotations of the tetrahedra about $\mathbf{c}_p$ through the centre of the tetrahedra as shown in Fig. 2a. The sense of rotation from one tetrahedral layer to the next within the same double tetrahedral layer, however, is now constrained to be of opposite sign, as shown in Fig. 2b.

Application to Ba-hexacelsian

The existence of a second quite distinct type of RUM which is soft at any particular modulation wave vector provides a crucial extra degree of freedom when attempting to explain the experimentally observed behaviour of hexacelsians in general, and Ba-hexacelsian in particular. Specifically, it allows for the possibility of more than one tetrahedral rotation pattern being associated with any modulation wave vector perpendicular to $\langle 110 \rangle$.

The non-disappearance of the $\mathbf{G} \pm 1/2\langle\bar{1}101\rangle^*$ type satellite reflections on heating up through the α to β phase transition (see Fig. 3), coupled with the sudden appearance of the characteristic diffuse distribution associated with the first type of RUM, implies that the atomic shifts associated with $\mathbf{q} = 1/2[\bar{1}101]^*$ above the phase transition are not due to a type I RUM but can only be due to a condensed RUM of type II, as shown in Fig. 5. The associated atomic shifts for this RUM are all perpendicular to the $\langle\bar{1}10\rangle$ rotation axis and involve basal plane motion along $\langle 110 \rangle$ as well as c axis shifts. Given a $P6/mmm$ parent structure, a condensed phonon mode of wave vector $\mathbf{q} = 1/2[\bar{1}101]^*$ and with the symmetry of the type II RUM (an R_4 irreducible representation; see Table 2) would lead to a resultant orthorhombic structure of space group *Ibmm* ($\mathbf{a}_o = \mathbf{a} + \mathbf{b}, \mathbf{b}_o = -\mathbf{a} + \mathbf{b}, \mathbf{c}_o = 2\mathbf{c}$). [Given a $P6/mmm$ parent structure, the little cogroup, $\bar{G}^q$, for $\mathbf{q} = 1/2[\bar{1}101]^*$ is given by $\bar{G}^q = \{E, C_2, C''_{23}, C'_{23}, \ i, m_h, iC''_{23}, iC'_{23}\}$ in the notation of Bradley and Cracknell (1972). The eight corresponding irreducible representations, together with the resultant space group symmetry given a condensed phonon mode of that symmetry, are listed in Table 2].

Table 2 Irreducible representations associated with the little cogroup of the modulation wave vector $\mathbf{q} = 1/2[\bar{1}101]^*$

	E	C_2	C''_{23}	C'_{23}	i	m_h	iC''_{23}	iC'_{23}	Space group	No.
	E	C_{2z}	C_{2x}	C_{2y}	i	m_z	m_x	m_y		
R_1	1	1	1	1	1	1	1	1	*Immm*	71
R_2	1	−1	1	−1	1	−1	1	−1	*Imam*	74
R_3	1	1	−1	−1	1	1	−1	−1	*Ibam*	72
R_4	1	−1	−1	1	1	−1	−1	1	*Ibmm*	74
R_5	1	1	1	1	−1	−1	−1	−1	*Ibam*	72
R_6	1	−1	1	−1	−1	1	−1	1	*Ibmm*	74
R_7	1	1	−1	−1	−1	−1	1	1	*Immm*	71
R_8	1	−1	−1	1	−1	1	1	−1	*Imam*	74

The symmetry elements of the little group with respect to the parent $P6/mmm$ hexagonal unit cell are given in the *first row*. The equivalent symmetry operations with respect to the $\mathbf{a}_o = \mathbf{a} + \mathbf{b}$, $\mathbf{b}_o = -\mathbf{a} + \mathbf{b}$, $\mathbf{c}_o = 2\mathbf{c}$ resultant cell are given in the *second row* (cf. Fig. 6). The space group symmetry resulting from condensed modes transforming according to each irreducible representation are given in *column 10*

Unfortunately, the layered nature of hexacelsians (the normal to the plates is always parallel to **c**) in conjunction with the limited tilt facilities of TEM hot stages rules out the possibility of confirming the presence or otherwise of the predicted b glide perpendicular to a_o. Nonetheless, the fact that the $\mathbf{G} \pm 1/2\langle\bar{1}101\rangle^*$ type satellite reflections in the first-order Laue zone (FOLZ) ring of the close to [0001] zone axis EDP of Fig. 3b are transverse polarized, i.e. most intense along the $\langle 110 \rangle$ direction (orthogonal to the modulation wave vector $1/2\langle\bar{1}101\rangle^*$) is entirely compatible with the predicted atomic displacement pattern shown in Fig. 5. By contrast, this experimental observation is incompatible with the *Immm* space group symmetry for the β phase suggested by Müller (1977). (A character of +1 under m_x, for example, as required by a resultant space group symmetry of *Immm* – see Table 2 – constrains all metal atoms to move perpendicular, rather than parallel, to $\langle 110 \rangle$).

The sudden disappearance of the characteristic diffuse distribution associated with the first type of RUM on cooling through the β to α phase transition of stoichiometric Ba-hexacelsian implies the freezing-in of an additional soft phonon mode characterized by a modulation wave vector perpendicular to $\langle 110 \rangle$ and with a displacement eigenvector of the type shown in Fig. 4a. Given that the only satellite reflections observed in both the α and β phases, in addition to the strong Bragg reflections, **G**, characteristic of the underlying parent structure (Tabira et al. 2000), are of $\mathbf{G} \pm 1/2\langle\bar{1}101\rangle^*$ type, there are only two possible choices for the modulation wave vector of a frozen in RUM mode of this type, i.e. $\mathbf{q} = 1/2[\bar{1}101]^*$ or $\mathbf{q} = \mathbf{0}$.

The atomic displacement pattern associated with a type I, $\mathbf{q} = 1/2[\bar{1}101]^*$ RUM is shown in Fig. 4b for a

particular double tetrahedral layer. It corresponds to an R_5 irreducible representation (see Table 2) and, on its own, would lead to a resultant orthorhombic structure of space group *Ibam* ($\mathbf{a}_o, \mathbf{b}_o, \mathbf{c}_o$). (Note that the $1/2\mathbf{c}^*$ component of this modulation wave vector requires that the displacements shown in Fig. 4b reverse from one double tetrahedral layer to the next along the *c* direction). Given that a type II, $\mathbf{q} = 1/2[\bar{1}101]^*$ RUM mode has already condensed out in the high-temperature β polymorph, the space group symmetry for the low-temperature α polymorph would be determined by the combination of the two (type I and II) RUM modes. Simultaneously condensed type I and II, $\mathbf{q} = 1/2[\bar{1}101]^*$ RUM modes lead to a resultant orthorhombic structure of space group symmetry *Ib*2*m* ($\mathbf{a}_o, \mathbf{b}_o, \mathbf{c}_o$). The corresponding fractional co-ordinates are listed in Table 3. (For examples of how to derive resultant fractional co-ordinates from condensed RUMs see, for example, Withers et al. 1997; Thompson et al. 1998a, b).

The atomic displacement pattern for a type I RUM associated with the alternate modulation wave vector possibility, i.e. $\mathbf{q} = \mathbf{0}$, is in essence the same as that shown in Fig. 2a where the two tetrahedral layers of each double tetrahedral layer are understood to rotate in the same sense (as opposed to the type III, $\mathbf{q} = \mathbf{0}$, RUM mode where they are understood to rotate in the opposite sense; see Fig. 2b). On its own, a $\mathbf{q} = \mathbf{0}$ RUM mode of type I would lead to a resultant space group symmetry of $P\bar{6}2m$ (**a**, **b**, **c**) (ignoring for the moment Al/Si ordering and concentrating purely on the tetrahedral rotation component of Fig. 2a). Note that ditrigonal cavities are formed in the case of such $\mathbf{q} = \mathbf{0}$ modes whereas elliptical-shaped cavities are formed in the case of the $\mathbf{q} = 1/2[\bar{1}101]^*$ mode (cf. Fig. 4b with Fig. 2a. Simultaneously condensed $\mathbf{q} = \mathbf{0}$, type I (see Fig. 2a) and $\mathbf{q} = 1/2[\bar{1}101]^*$, type II RUM modes lead to a resultant orthorhombic structure of space group symmetry *I*2*mm* ($\mathbf{a}_o, \mathbf{b}_o, \mathbf{c}_o$) (ignoring again Al/Si ordering and concentrating purely on the tetrahedral rotation modes).

The third, and final, possibility for the tetrahedral rotation around the **c** component of the overall distortion is a $\mathbf{q} = \mathbf{0}$, type III RUM mode of the type proposed by Kremenovic et al. (1997) (see Fig. 2b). On its own, a $\mathbf{q} = \mathbf{0}$ RUM mode of this sort gives rise to a resultant space group symmetry of $P\bar{3}1m$ (**a**, **b**, **c**) (again ignoring Al/Si ordering and concentrating purely on the tetrahedral rotation component of Fig. 2b). A simultaneously condensed $\mathbf{q} = \mathbf{0}$ mode of this type in conjunction with a $\mathbf{q} = 1/2[\bar{1}101]^*$, type II RUM mode would this time lead to a resultant monoclinic structure of space group symmetry $I12/m1$ ($\mathbf{a}_o, \mathbf{b}_o, \mathbf{c}_o$).

Crystal chemical considerations

At this stage, there exist three potential candidates for the condensed RUM involving tetrahedral rotation around **c** but a single unique candidate for the type II RUM involving tetrahedral rotation around $[\bar{1}10]$. The question is which of the three potential candidates for the condensed RUM involving tetrahedral rotation around **c** is correct and what are the magnitudes of the corresponding tetrahedral rotation angles.

The magnitude of the tetrahedral rotation around **c** mode might reasonably be expected to be $\sim 10^\circ$ given the rather similar "average structure" refinement results of Takéuchi (1958) and Kremenovic et al. (1997). Takéuchi (1958), for example, gives the (disordered) O(2) basal plane oxygen position as (1/2 + 0.05, 0, 0.209). The deviation of 0.05**a** from the ideal *P*6/*mmm* position corresponds to a tetrahedral rotation around **c** $\sim 9.8^\circ$. Kremenovic et al. (1997), on the other hand, give the O(2) position as $(0 - 0.0252, 1/2 - 0.0655, 0.21)$ in space group $P\bar{3}$. This fractional coordinate can be rewritten as $(0, 1/2, 0.21) + (0, -0.0529, 0) + (-0.0252, -0.0126, 0)$ with the second term giving the purely rotational RUM contribution and the latter the expansion/contraction contribution due to Al/Si ordering. A shift of 0.0529**b** from the ideal *P*6/*mmm* position corresponds to a tetrahedral rotation around **c** $\sim 10.4^\circ$ in reasonably good agreement with Takéuchi (1958), despite the different space group symmetries employed to describe the tetrahedral rotation.

Tetrahedral rotation around **c** of magnitude $\sim 10^\circ$ will obviously expand the size of the TO_4 tetrahedra and hence reduce the overbonding of the T atoms (cf. Table 1b with Table 1a). In addition, it leads to a change in the coordination environment of the Ba ions between the double tetrahedral layers and a general improvement in the underbonding of the Ba ions. Nonetheless, the T ions still remain overbonded (by ~ 0.2 valence units) and the Ba ions significantly underbonded (by ~ 0.4 valence

Table 3 Proposed fractional coordinates in space group *Ib*2*m* ($\mathbf{a}_o = \mathbf{a} + \mathbf{b}$, $\mathbf{b}_o = -\mathbf{a} + \mathbf{b}$, $\mathbf{c}_o = 2\mathbf{c}$) as a function of rotation angle around $[\bar{1}10]$, R_y (see Fig. 6) and rotation angle around **c**, R_z (see Fig. 4b)

	X_o	Y_o	Z_o
Ba	0.0	0.0	0.0
T1	0.1115 R_y + 0.2887 R_z	0.3333	0.1453
T2	0.1115 R_y − 0.2887 R_z	0.6666	0.1453
O1	0.4197 R_y + 0.2887 R_z	0.3333	0.2500
O2	0.4197 R_y − 0.2887 R_z	0.6666	0.2500
O3	0.0	0.5	0.1075
O4	0.25 + 0.4330 R_z	0.25 + 0.1443 R_z	0.1075 − 0.0849 R_y
O5	0.75 + 0.4330 R_z	0.25 − 0.1443 R_z	0.1075 + 0.0849 R_y

The coefficients of the various terms simply reflect the relative distance from the rotation axis to the relevant atom

units – see Table 1b). It is clear that the tetrahedral rotation around $[\bar{1}10]$ mode is also needed in order to satisfy local crystal chemistry.

It turns out that it is possible to obtain correctly sized TO_4 tetrahedra via an appropriate combination of any one of the rotation around **c** modes with the $\mathbf{q} = 1/2[\bar{1}101]^*$, type II RUM mode. It is not, however, possible to simultaneously improve the underbonding of all Ba ions via a combination of either of the $\mathbf{q} = \mathbf{0}$ rotation around **c** modes with the $\mathbf{q} = 1/2[\bar{1}101]^*$, type II RUM mode. In both cases, whatever the sense or magnitude of the rotations, there are always two crystallographically distinct Ba ions formed. The calculated valences (AVs) for these Ba ions are found to always move in opposite directions with respect to an (already initially under-bonded) average value ~1.6 if either of the $\mathbf{q} = \mathbf{0}$ rotation around **c** modes are used.

If, on the other hand, the $\mathbf{q} = 1/2[\bar{1}101]^*$, type I RUM mode is used for the tetrahedral rotation around **c** component of the overall distortion, only one crystallographically distinct Ba ion is formed whose valence can be adjusted to a crystal chemically very reasonable value via a combination of a 15.76° rotation around **c** combined with a 7.88° rotation around $[\bar{1}10]$ (see the fractional coordinates listed in Table 3 and the apparent valences of Table 4a). The average metal ion to oxygen distance within each tetrahedra is then 1.69 Å (exactly midway between the 1.624 Å expected for an Si-O distance and the 1.757 Å expected for an Al-O distance) with a spread of only ~0.02 Å. (Note that the various possible sign combinations of the rotations do not generate distinct structures but are simple twins of the original structure). We therefore believe, on general crystal chemical grounds, that the tetrahedral rotation around **c** mode must be associated with the $\mathbf{q} = 1/2[\bar{1}101]^*$, type I RUM mode. Certainly the fractional coordinates generated from Table 3 using $R_y = 0.1375$ radians (7.88°) and $R_z = 0.275$ radians (15.76°) represent a crystal chemically plausible structure, both in terms of apparent valences (see Table 4a) as well as in having non-linear T-O-T bond angles along the c_p axis.

Table 4 **a** Calculated bond valence sums (AVs) for the proposed *Ib*2*m* ($\mathbf{a}_o = \mathbf{a} + \mathbf{b}$, $\mathbf{b}_o = -\mathbf{a} + \mathbf{b}$, $\mathbf{c}_o = 2\mathbf{c}$) structure

	Ba	T(1)	T(2)	O(1)	O(2)	O(3)	O(4)	O(5)
AV (T = Al)	1.986	3.635	3.638	2.014	2.014	1.990	2.249	2.013
AV (T = Si)	1.986	3.379	3.382	1.872	1.872	1.864	2.127	1.890
Average AV	1.986	3.507	3.510	1.943	1.943	1.927	2.188	1.952
Expected AV	2.0	3.5	3.5	2.0	2.0	2.0	2.0	2.0

Coordinates from Table 3 with $R_y = 0.1375$ radians and $R_z = 0.275$ radians

b Calculated bond valence sums (AVs) for the final proposed *Ib*11 ($\mathbf{a}_o = \mathbf{a} + \mathbf{b}$, $\mathbf{b}_o = -\mathbf{a} + \mathbf{b}$, $\mathbf{c}_o = 2\mathbf{c}$) Al/Si ordered structure

	AV	Expected AV
Ba	1.940	2.0
Al(1)	3.089	3.0
Si(1)	3.968	4.0
Si(2)	4.026	4.0
Al(2)	3.065	3.0
O(1)	1.964	2.0
O(2)	1.964	2.0
O(3)	1.939	2.0
O(3)′	1.910	2.0
O(4)	2.154	2.0
O(4)′	2.201	2.0
O(5)	2.001	2.0
O(5)′	1.957	2.0

Coordinates from Table 4 with $R_y = 0.1375$ radians, $R_z = 0.275$ radians, $\varepsilon_T = 0.045$ and $\varepsilon_b = 0.01$

Al/Si ordering and associated structural relaxation

The Al/Si ordering found recently to exist in the α phase (of Ba-hexacelsian synthesized from zeolite precursors: Dondur et al. 1995) can be taken into account by an additional $P\bar{3}m1$, $\mathbf{q} = \mathbf{0}$ Al/Si ordering mode superimposed on top of the *Ib*2*m* fractional coordinates of Table 3. The addition of such a mode, however, automatically reduces the resultant space group symmetry from *Ib*2*m* to *Ib*11. The associated expansion/contraction of the AlO_4 and SiO_4 tetrahedra gives rise to the fractional coordinate changes shown in Table 5. Choosing the additional fractional coordinate parameters $\varepsilon_T = 0.045$ and $\varepsilon_b = 0.010$ gives rise to an extremely plausible resultant Al/Si ordered structure (see the AVs of Table 4b) with average Al-O and Si-O bond lengths very close to the ideal 1.757 and 1.624 Å and with a small spread (~0.02–0.03 Å).

Conclusions

The picture of Ba-hexacelsian that has thus finally emerged is of an ideal *P*6/*mmm* (**a**, **b**, **c**) parent structure ($P\bar{3}m1$ if Al/Si ordering and associated expansion/contraction of tetrahedra is taken into account) characterized by dynamically excited RUM modes at high temperature which first of all transforms (at some unknown temperature above the ~310 °C α to β phase transition) via the condensation of a $\mathbf{q} = 1/2[\bar{1}101]^*$, type II RUM mode to an *Ibmm* ($\mathbf{a}_o = \mathbf{a} + \mathbf{b}, \mathbf{b}_o = -\mathbf{a} + \mathbf{b}, \mathbf{c}_o = 2\mathbf{c}$) β phase characterized by dynamically excited type I RUM modes followed by a subsequent β to α phase transition at which a $\mathbf{q} = 1/2[\bar{1}101]^*$, type I RUM mode also condenses out, leading to a resultant α phase orthorhombic structure of space group symmetry *Ib*2*m* ($\mathbf{a}_o, \mathbf{b}_o, \mathbf{c}_o$; space group symmetry *Ib*11 if Al/Si ordering is taken into account). The dynamically excited RUM modes at high temperature, like the related silica polymorphs, could be expected to add together in such a way that T-O-T bond angles are always non-linear at any instant of time while appearing linear on average (see, for example, Hammonds et al. 1996).

Table 5 Final proposed Al/Si ordered fractional coordinates in space group *Ib*11 ($\mathbf{a}_o = \mathbf{a} + \mathbf{b}$, $\mathbf{b}_o = -\mathbf{a} + \mathbf{b}$, $\mathbf{c}_o = 2\mathbf{c}$) as a function of rotation angle around $[\bar{1}10]$, R_y, rotation angle around **c**, R_z and the two relaxation parameters, ε_T and ε_b describing the expansion/contraction of the AlO_4 and SiO_4 tetrahedra

	X_o	Y_o	Z_o
Ba	0.0	0.0	0.0
Al(1)	$0.1115\ R_y + 0.2887\ R_z$	0.3333	$0.1453 - \varepsilon_T$
Si(1)	$0.1115\ R_y + 0.2887\ R_z$	0.3333	$0.3547 - \varepsilon_T$
Si(2)	$0.1115\ R_y - 0.2887\ R_z$	0.6666	$0.1453 + \varepsilon_T$
Al(2)	$0.1115\ R_y - 0.2887\ R_z$	0.6666	$0.3547 + \varepsilon_T$
O1	$0.4197\ R_y + 0.2887\ R_z$	0.3333	0.2500
O2	$0.4197\ R_y - 0.2887\ R_z$	0.6666	0.2500
O3	0.0	$0.5 + \varepsilon_b$	0.1075
O3′	0.0	$0.5 - \varepsilon_b$	0.3925
O4	$0.25 + 0.4330\ R_z + 3/2\varepsilon_b$	$0.25 + 0.1443\ R_z - 1/2\varepsilon_b$	$0.1075 - 0.0849\ R_y$
O4′	$0.25 + 0.4330\ R_z - 3/2\varepsilon_b$	$0.25 + 0.1443\ R_z + 1/2\varepsilon_b$	$0.3925 + 0.0849\ R_y$
O5	$0.75 + 0.4330\ R_z - 3/2\varepsilon_b$	$0.25 - 0.1443\ R_z - 1/2\varepsilon_b$	$0.1075 + 0.0849\ R_y$
O5′	$0.75 + 0.4330\ R_z + 3/2\varepsilon_b$	$0.25 - 0.1443\ R_z + 1/2\varepsilon_b$	$0.3925 - 0.0849\ R_y$

Acknowledgements The award of an Australian Research Council (ARC) postdoctoral fellowship to Y.T. is gratefully acknowledged. Most of this work was carried out while R.W. was visiting the Departamento de Fisica de la Materia Condensada, Universidad del Pais Vasco, Bilbao, Spain as Profesor Visitante Iberdrola. Iberdrola is gratefully acknowledged for financial support.

References

Bradley CJ, Cracknell AP (1972) The mathematical theory of symmetry in solids. Clarendon, Oxford

Brese NE, O'Keeffe M (1991) Bond-valence parameters for solids. Acta Cryst B47: 192–197

Dimitrijevic R, Kremenovic A, Dondur V, Tomasevic-Canovic M, Mitrovic M (1997) Thermally induced conversion of Sr-exchanged LTA- and FAU-framework zeolites. Syntheses, characterization and polymorphism of ordered and disordered $Sr_{1-x}Al_{2-2x}Si_{2+2x}O_8$ ($x = 0$; 0.15), diphyllosilicate, and feldspar phases. J Phys Chem 101: 3931–3936

Dondur V, Dimitrijevic R, Kremenovic A, Mioc U, Srejic M, Tomasevic-Canovic M (1995) Structural characterization of hexagonal $Ba_{1-x}Al_{2-2x}Si_{2+2x}O_8$ phases synthesized from zeolite precursors. In: Vincenzini P (ed) Adv Sci Technol 3, Part B, Techna, Faenza, Italy, pp 687–694

Dove MT, Heine V, Hammonds KD, Gambhir M, Pryde AKA (1998) Short range disorder and long-range order: implications of the Rigid Unit Mode model. In: Billinge SJL, Thorpe MF (eds) Local structure from diffraction. Plenum Press, New York, pp 253–271

Gibbs GV, Meagher EP, Newton MD, Swanson DK (1981) A comparison of experimental and theoretical bond length and angle variations for minerals, inorganic solids, and molecules. In: O'Keeffe M, Navrotsky A (eds) Structure and bonding in crystals I, Academic Press, New York, pp 195–225

Hammonds KD, Dove MT, Giddy AP, Heine V (1994) Crush: a fortran program for the analysis of the rigid-unit mode spectrum of a framework structure. Am Mineral 79: 1207–1209

Hammonds KD, Dove MT, Giddy AP, Heine V, Winkler B (1996) Rigid-unit modes and structural phase transitions in framework silicates. Am Mineral 81: 1057–1079

Ito T (1950) X-ray studies on polymorphism. Maruzen, Tokyo

Kremenovic A, Norby P, Dimitrijevic R, Dondur V (1997) Time-temperature resolved synchrotron XRPD study of the hexacelsian α-β polymorph inversion. Solid State Ionics 101–103: 611–618

Kremenovic A, Norby P, Dimitrijevic R, Dondur V (1997) High-temperature synchrotron powder diffraction investigation of thermal expansion, strain and microstructure for the coelastic $\alpha \leftrightarrow \beta$ hexacelsian transition. Phase Transitions 68: 587–605

Liebau, F (1985) Structural chemistry of silicates. Springer, Berlin Heidelberg New York

Loewenstein W (1954) The distribution of aluminum in the tetrahedra of silicates and aluminates. Am Mineral 39: 92–96

Müller WF (1977) Phase transitions and associated domains in hexacelsian ($BaAl_2Si_2O_8$). Phys Chem Miner 1: 71–82

Oehlschlegel G, Kockel A, Biedl A (1974) Anisotrope Wärmedehnung und Mischkristallbildungeiniger Verbindungen des ternären Systems BaO-Al_2O_3-SiO_2, parts 1 und 2. Glastech Ber 44: 24–41

Oehlschlegel G, Abraham K, Flörke OW (1976) Das Kristallwachstum von $BaAl_2Si_2O_8$. Krist U Techn 11: 59–72

Pentinghaus H (1975) Hexacelsiane. Fortsch Miner 53 (Suppl.1): 65–66

Schadt J, Müller WF, Pentinghaus H (1976) Transmissionselektronenmikroskopische Untersuchungen an $SrAl_2Si_2O_8$. Abst. 16. Diskussionstag Arbeitsgem Kristallogr. Braunschweig, Sept 14–17

Tabira Y, Withers RL, Takéuchi Y, Marumo F (2000) Structured diffuse scattering, displacive flexibility and polymorphism in Ba-hexacelsian. Phys Chem Mineral 27: 194–202

Takéuchi Y (1958) A detailed investigation of the structure of hexagonal $BaAl_2Si_2O_8$ with reference to its α-β inversion. Mineralog J 2: 311–332

Takéuchi Y, Donnay G (1959) The crystal structure of hexagonal $CaAl_2Si_2O_8$. Acta Crystallogr 12: 465–470

Thompson JG, Withers RL, Melnitchenko A, Palethorpe SR (1998a) Cristobalite-related phases in the $NaAlO_2$-$NaAlSiO_4$ system. I. Two tetragonal and two orthorhombic structures. Acta Crystallogr B54: 531–546

Thompson JG, Withers RL, Palethorpe SR, Melnitchenko A (1998b) Cristobalite-related oxide structures. J Solid State Chem 141: 29–49

Toepel-Schadt J, Müeller WF, Pentinghaus H (1978) Transmission electron microscopy of strontium aluminium silicate ($SrAl_2Si_2O_8$). Feldspar and hexacelsian polymorphs. J Mater Sci 13: 1809–1816

Withers RL, Lobo C, Thompson JG, Schmid S, Stranger R (1997) A modulation wave approach to the structural characterization of three new cristobalite-related sodium magnesiosilicates. Acta Crystallogr B53: 203–220